ACS OMEGA

Open Access

http://pubs.acs.org/journal/acsodf

Article

Near-Infrared Light-Mediated Antibacterial Photodynamic Therapy Based on Erythrosine-Functionalized Mesoporous Silica-Coated Upconversion Nanoplatform

Jing Luo,[#] Hui Zhang,[#] and Qingqing Chen*

Cite This: *ACS Omega* 2024, 9, 34799−34807

Read Online

ACCESS | Metrics & More | Article Recommendations | Supporting Information

ABSTRACT: Infectious diseases caused by bacteria pose a serious threat to public health, and more worryingly, the unregulated application of antibiotics accelerates the emergence of bacterial resistance, presenting a major challenge to the effective treatment of infectious diseases caused by bacteria. Therefore, there is an urgent necessity to develop efficient and safe antimicrobial systems. Photodynamic therapy (PDT) is an attractive therapeutic approach that does not induce bacterial resistance. However, the clinical application of PDT has been limited by several factors, including the lower tissue penetration depth of photoactivation under visible light irradiation and the uncertain biosafety of photosensitizers (PS). This work presents an near infrared (NIR)-triggered core−shell upconversion nanoparticle-based PDT system composed of mesoporous silica-coated lanthanide-doped upconversion nanoparticles loaded with the photosensitizer erythrosine (UCSE). Upon NIR-triggering, erythrosine generates highly efficient reactive oxygen species that disrupt the cell membranes of *Staphylococcus aureus* and *Escherichia coli*, exhibiting a potent photodynamic antimicrobial effect. It is worth noting that the UCSE also exhibits excellent biosafety. In conclusion, we present an efficient NIR-triggered nanoantimicrobial system with excellent antimicrobial capacity and biosafety, which is a new therapeutic strategy for the control of bacterial infectious diseases.

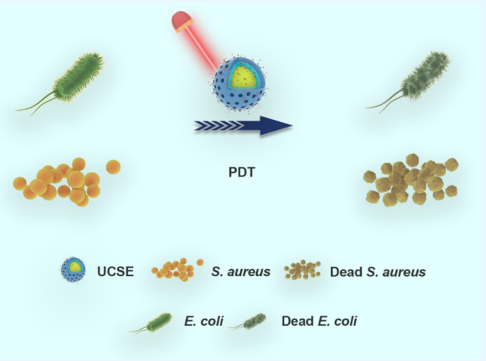

INTRODUCTION

Bacterial infectious diseases, such as infected wounds, periodontal disease, and even bacteremia, pose a serious threat to human health, resulting in approximately 700,000 deaths worldwide each year due to serious complications.[1] Antibiotics are widely used to treat bacterial infections. However, their inappropriate application and overuse have led to the development of bacterial resistance, and these resistant bacteria are more difficult to treat.[2−5] In recent years, many antibiotic-independent antimicrobial methods have been developed, such as biologically active substance-based antimicrobial therapy, photothermal therapy (PTT), and photodynamic therapy (PDT) modalities.[6−9] PTT is a noninvasive therapeutic method for antimicrobial treatment by converting absorbed light energy into heat energy through photothermal materials.[10] However, the high temperatures (>50 °C) at which photothermal effectively sterilizes bacteria inevitably cause damage to the surrounding normal tissues.[9] Photodynamic antimicrobial therapy utilizes specific wavelengths of light to excite photosensitizers (PS) from the ground state to the excited state, causing the release of large amounts of reactive oxygen species (ROS), such as superoxide anions ($O_2^{\bullet-}$), hydroxyl radicals ($^{\bullet}OH$), and singlet oxygen ($^1O_2$), which disrupt the bacterial cell membranes and DNA, and thus induce bacterial death in a nonselective manner.[11−13] The nonspecific antimicrobial mechanism of action of PDT is less likely to induce the development of bacterial drug resistance,[14,15] and therefore, PDT has received considerable attention from researchers.

Although PDT is considered a noncontact and minimally invasive effective treatment modality for localized microbial infections,[16] inherent challenges remain. Currently, the excitation light of the major molecular PS is located in the high-energy short-wave ultraviolet−visible region (400−700 nm), and the tissue penetration of such sources is insufficient, limiting their application to deep lesions.[17,18] While the excitation light located in the low-energy near-infrared region (750−2000 nm) could penetrate deeply into tissues,[19,20] most PS molecules are less sensitive to the near-infrared and could not produce satisfactory antimicrobial effects, which greatly limits the clinical application of PDT.[21] To solve this issue, rare earth ions (Tm^{3+}, Yb^{3+}, and Er^{3+}) with unique step energy layer structures were doped into upconverted nanoparticles,

Received: May 6, 2024
Revised: June 16, 2024
Accepted: July 24, 2024
Published: July 31, 2024

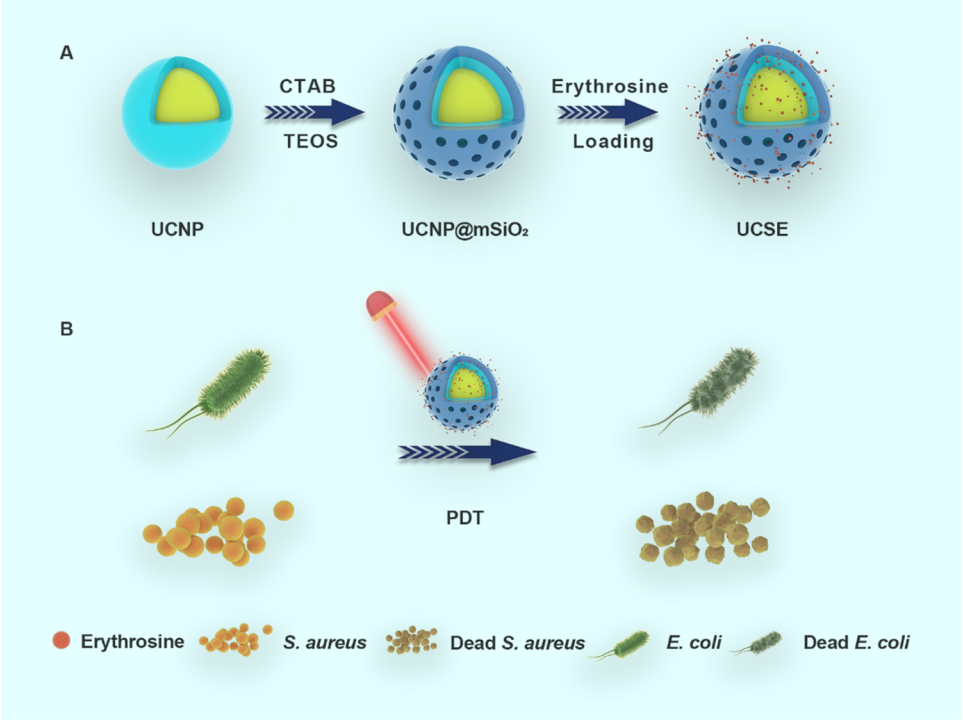

Figure 1. Schematic illustrations of UCSE synthesis (A) and the therapeutic procedure of the NIR-mediated antibacterial photodynamic therapy (B).

which can convert longer wavelengths of near-infrared light into shorter wavelengths of the ultraviolet (UV) and visible regions through a nonlinear process,[22,23] thus providing the possibility of a photoresponsive PDT antimicrobial system that penetrates deeply into tissues.[24,25]

Erythrosine is a dye approved by the FDA for food products and has been approved for dental use with excellent biosafety.[26] Erythrosine acts as a photosensitizer derived from a xanthine moiety with an absorption range of 500−550 nm.[27] Recent studies have shown that erythrosine as a photosensitizer displays inhibitory effects on cancer cells[28] and antimicrobial potential against *Streptococcus pyogenes* and *Candida albicans*.[29,30] However, the short excitation wavelength limits its clinical application.

To address these limitations, a PDT antimicrobial platform based on near infrared (NIR) excitation was designed and synthesized in this work. As shown in Figure 1A, first, we synthesized upconversion nanoparticles (UCNP) with a core−shell structure, which possesses the ability to convert NIR light to shorter wavelengths of UV and visible light. Next, the UCNP were coated with mesoporous silica ($mSiO_2$), and the mesoporous structure of $mSiO_2$ was used to load erythrosine as a PDT photosensitizer. This novel platform UCSE was able to provide an antibacterial effect through its inhibition of bacterial metabolism by NIR excitation, where visible fluorescence from the UCNP triggered the loaded erythrosine, which interacted with the surrounding basal molecular oxygen to produce the $^1O_2$ state of oxygen. The above results indicate that this NIR-stimulated UCSE nanocomposite drug-carrying system provides a promising approach in addressing the therapeutic problem of bacterial infectious diseases and has favorable application prospects.

MATERIALS AND METHODS

Materials. Yttrium(III) chloride hexahydrate ($YCl_3·6H_2O$), ytterbium(III) chloride hexahydrate ($YbCl_3·6H_2O$), erbium(III) chloride hexahydrate ($ErCl_3·6H_2O$), ammonium fluoride, oleic acid, (3-aminopropyl) triethoxysilane (APTES), ammonium fluoride(NH_4F), and 1,3-diphenylisobenzofuran (DPBF) were purchased from Aladdin. Calcein acetoxymethyl ester (calcein AM) (solubilized in dimethyl sulfoxide (DMSO)), propidium iodide (PI), ammonium nitrate (NH_4NO_3), and hexadecyltrimethylammonium bromide (CTAB) were procured from Sigma-Aldrich. Dulbecco's modified Eagle's medium (DMEM), penicillin/streptomycin, and fetal bovine serum (FBS) were acquired from Gibco. Cell Counting Kit-8 (CCK-8) was purchased from BioMake.

Preparation of UCNP@ $mSiO_2$@Erythrosine(UCSE). *UCNP.* In a typical synthesis of $NaYF_4$:Yb,Er,[31] $YCl_3·6H_2O$ (485.4 mg), $YbCl_3·6H_2O$ (139.5 mg), and $ErCl_3·6\ H_2O$ (76.3 mg) were added to a flask containing oleic acid (15 mL) and 1-octadecadienne (30 mL), and the mixture was stirred for 1 h at room temperature. The mixture was then slowly heated to 120 °C under an inert gas atmosphere and kept at 156 °C for about 1 h until a homogeneous, clear yellow solution was obtained. After cooling to room temperature, 10 mL of a methanol solution containing NH_4F (296.3 mg) and NaOH (200 mg) was added and stirred for 2 h. After that, it was heated to 290 °C and kept for 1.5 h. After cooling to room temperature, 20 mL of ethanol was added, and the mixture was collected by centrifugation at 10,000 r min^{-1} for 10 min. After the sample was washed 4 times using cyclohexane with ethanol, the final product was redispersed in cyclohexane (20 mL).

For the synthesis of $NaYF_4$:Yb,Er@$NaYF_4$ (UCNP), $NaYF_4$:Yb,Er (1.0 mmol) and $YCl_3·6H_2O$ (800 μmol) were added to a flask containing oleic acid (15 mL) and 1-octadecadienne (30 mL), stirred for 1 h at room temperature,

https://doi.org/10.1021/acsomega.4c04310
ACS Omega 2024, 9, 34799−34807

and the mixture was heated slowly under a nitrogen atmosphere to 156 °C. It was kept for about 1 h until a homogeneous clear yellow solution was obtained. The system was then cooled to room temperature under a stream of argon, 5 mL of $NaYF_4$:Yb,Er was added, stirred at room temperature for 30 min, and then heated to 80 °C to remove cyclohexane. 10 mL of methanol solution containing 1 mmol of NH_4F and 1.685 mmol of NaOH was added and stirred at room temperature for 2 h. After that, the solution was heated to 280 °C for 1.5 h, then cooled to room temperature and washed by centrifugation to collect the nanoparticles.

UCNP@mSiO$_2$. Mesoporous silica shells were synthesized around upconverted nanoparticles using the reported methods.[32] 4 mL of ethanol solution containing 20 mg of UCNP was mixed with 200 mg of CTAB and 40 mL of water, which was vigorously stirred at room temperature for 12 h. 20 mL of the above solution was added to a mixture of 40 mL of water, 6 mL of ethanol, and 300 μL of NaOH (2 M) solution, heated to 70 °C, and 0.4 mL of tetraethyl orthosilicate (TEOS) was added dropwise to allow the reaction to proceed for 10 min. The mixture was centrifuged and washed 3 times with ethanol. CTAB was removed by ion-exchange method, and 20 mg of the synthesized UCNP@ $mSiO_2$ was transferred into 50 mL of ethanol containing 300 mg of NH_4NO_3 (3.75 mmol) and maintained at 60 °C for 2 h. The product was collected by centrifugal washing.

UCNP@mSiO$_2$@Erythrosine (UCSE). 150 mg of UCNP@ $mSiO_2$ nanoparticles was dissolved in a mixture of 20 mL of toluene and 50 mL of APTES. Under the protection of nitrogen, the mixture was stirred for 2 h, then centrifuged for 10 min, and the precipitate was collected. 50 mg of the above product was placed in 25 mL of ethanol containing 20 mg of erythrosine, and the reaction was stirred for 24 h at room temperature protected from light and centrifuged three times to obtain UCSE. When preparing UCSE, the unloaded erythrosine supernatant was collected by centrifugation, and the drug content in the solution was calculated by reading the absorbance of the supernatant. The drug loading rate of curcumin was calculated according to the following formula: drug loading rate = (mass of loaded erythrosine/mass of UCSE) × 100%.

Characterization. The morphology and structure of the samples were observed using a transmission electron microscope (TEM, Hitachi HT7800, Japan), and the solution absorbance of the nanoparticles (NPs) was measured by a UV−visible spectrometer (Shimadzu UV-2600, Japan). The upconversion luminescence properties of UCNP were measured by using a steady-state transient fluorescence spectrometer (FLS1000). The PDT effect of UCSE was irradiated by an NIR laser (808 nm laser, New Industries Optoelectronics Tech, Changchun, China).

Detection of ROS Generation. Next, we further investigated the ability of UCSE to generate ROS under NIR excitation using DPBF as the $^1O_2$ capture molecule.[33,34] A mixture of UCSE (0.5 mg/mL) and DPBF (1 mM) was exposed to 808 nm 1 W/cm^2 NIR light, and the generation of $^1O_2$ was detected by recording the UV−visible absorption spectra at different times of irradiation.

***In Vitro* Antimicrobial Effect.** In order to investigate the photodynamic bactericidal effect of UCSE nanoparticles on *Escherichia coli* and *Staphylococcus aureus*, the experiments were divided into the following four groups: (1) Phosphate-buffered saline (PBS); (2) NIR; (3) UCSE; and (4) NIR + UCSE. The final concentration of UCSE in the bacterial fluids of the final groups (3) and (4) was 500 μg/mL. Groups (2) and (4) were irradiated with an NIR-808 nm (W/cm^2) for 10 min. After the above treatments, they were incubated in an incubator for 20 min, protected from light. Plates were coated with equal dilutions of the bacterial mixtures of the four groups mentioned above followed by overnight incubation in the incubator, and the colonies were recorded with a camera. The number of colonies was counted, and the relative survival rate was calculated. The formula for calculating the relative survival rate of bacteria was as follows: relative survival rate of bacteria (%) = $N_t/N_c \times 100\%$, where N_t is the number of colonies in the experimental group and N_c indicates the number of colonies in the PBS group.

In addition, scanning electron microscope (SEM) was employed to observe the morphology of the bacteria. The procedure was as follows: the differently treated bacteria were collected by centrifugation at 4000 rpm for 5 min and immobilized in 2.5% glutaraldehyde solution at 4 °C for 12 h. The samples were dehydrated with different concentrations of ethanol solution in gradients (10, 30, 50, 70, 90, and 100%) for 10 min each. Finally, the bacterial morphology was observed by a scanning electron microscope (SEM).

Nanoparticles (final concentration of 500 μg/mL) were added to the *E. coli* and *S. aureus* bacterial fluids for coculture and treated with NIR-808 nm (1 W/cm^2) for 10 min. Bacteria treated with different treatments were collected, added with calcein AM and PI, and incubated for 20 min protected from light. After being washed by PBS, the dead and alive state of *E. coli* and *S. aureus* was observed under a fluorescence microscope and recorded to take state photographs.

Cytotoxicity Studies. Rat Schwann cell line (RSC96) was obtained from a commercial company. RSC96 were maintained in DMEM, which were supplemented with 10% FBS and 1% penicillin/streptomycin at 37 °C in 5% CO_2 atmosphere.

(1) The cytotoxicity of UCSE was determined by the CCK-8 method: RSC96 was diluted to 5×10^4 cells/mL and uniformly inoculated into 96-well plates with 100 μL per well. After overnight incubation, the medium was discarded, fresh complete medium was added to the blank control, and DMEM complete medium containing different concentrations (0, 0.0625, 0.125, 0.25, 0.5, 1, 2 mg/mL) of nanoparticles was added to the experimental group. After 1 and 2 days of incubation, respectively, the culture medium was discarded, the cells were washed three times with PBS, and 100 μL of DMEM containing 10% CCK-8 was added to each well. The incubation was continued for 2 h, and the absorbance at 450 nm was detected.

(2) Staining of live and dead cells: RSC96 was added to 96-well plates at 5×10^3 cells/well, and after cell walls adhered, it was added to complete culture medium with UCSE final concentrations of 0.25, 0.5, 1, and 2 mg/mL, and incubated for 24 h. Staining was performed according to the Calcein AM Cell Activity Assay Kit operating instructions, and representative pictures were obtained under a fluorescence microscope.

(3) Cytoskeleton staining: RSC96 was added to 24-well plates at 5×10^4 cells/well, and after 12 h, complete culture medium with UCSE final concentrations of 0.25, 0.5, 1, and 2 mg/mL was added and incubated for 24 h.

https://doi.org/10.1021/acsomega.4c04310
ACS Omega 2024, 9, 34799−34807

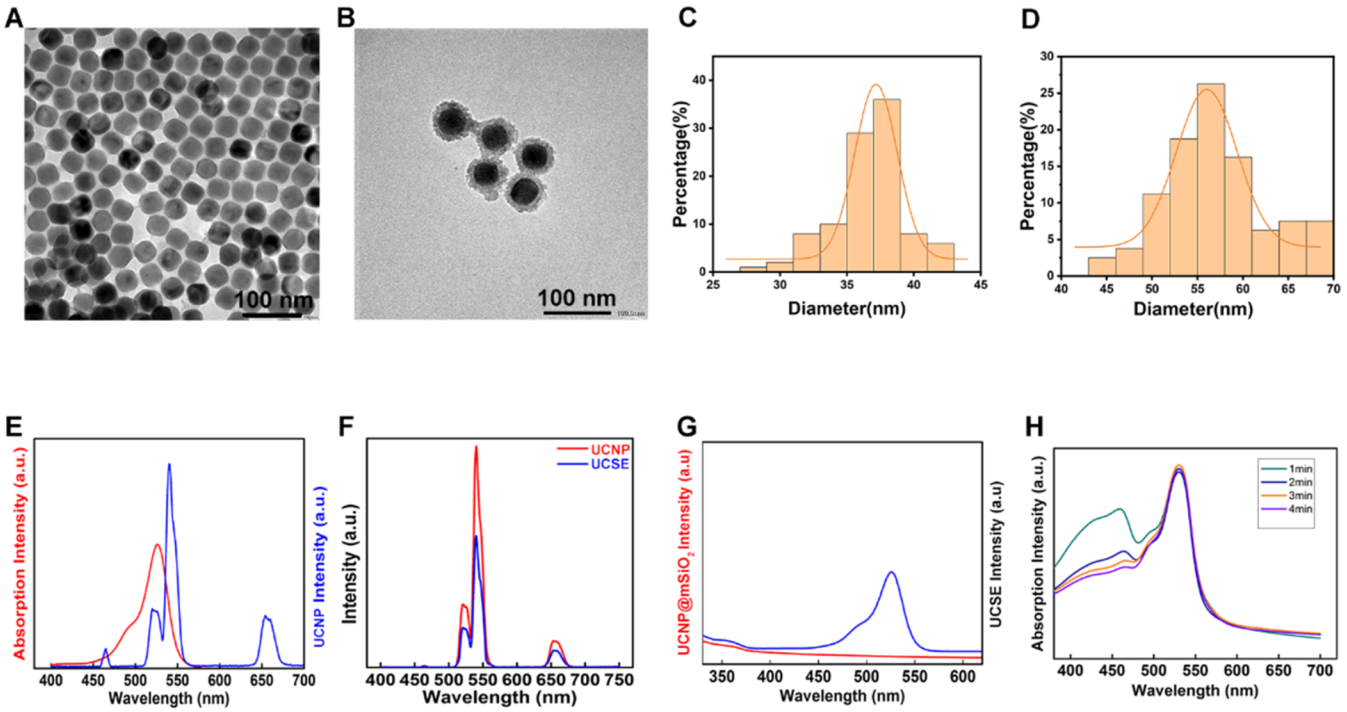

Figure 2. Characterization of NPs: (A, B) TEM images of UCNP and UCSE. Scale bar: 100 nm. (C, D) Graph of particle size distribution of UCNP and UCSE nanoparticles. (E) Emission fluorescence spectrum of UCNP excited at NIR-808 nm (blue line) and UV−visible spectrum of the photosensitizer of erythrosine (red line). (F) Fluorescence spectra of UCNP and UCSE under NIR-808 nm excitation. (G) UV−visible spectrum of UCSE (blue line) and UCNP@ $mSiO_2$ (red line). (H) UV−vis absorption spectra of DPBF after excitation with UCSE at NIR-808 nm.

Two milliliters of 4% paraformaldehyde was added and fixed for 30 min at room temperature. Subsequently, staining was performed according to the instructions of the phalloidin kit, and the results were observed under a fluorescence microscope.

Statistical Analysis. All results were expressed as means ± standard deviations. All statistical significance was conducted by one-way analysis of variance (ANOVA) for multiple comparisons (*P < 0.05, **P < 0.01, ***P < 0.001, ****P < 0.0001).

RESULTS AND DISCUSSION

Fabrication and Characterization of UCSE. The process of synthesizing UCSE and the therapeutic procedure of NIR-mediated PDT are shown in Figure 1A,B, respectively. The morphology of the synthesized products at each stage of the synthesis was first observed by TEM. Figure 2A shows the TEM of UCNP, and it can be seen that all of the nanoparticles are in monodisperse orthohexagonal morphology with a relatively uniform distribution. A very distinct core−shell structure can be seen in Figure 2B, where an $mSiO_2$ layer with a thickness of about 9.3 nm was uniformly generated on the surface of the nanoparticles with a clear mesoporous structure. Statistical analysis of the particle size showed that the average diameters of UCNP and UCSE were 36.6 and 56.7 nm, respectively (Figure 2C,D). A series of characterizations of the nanoparticles' properties were next performed; as shown in Figure 2E, there was a good overlap between the fluorescence emission of UCNP and the UV−vis absorption of erythrosine (525 to 545 nm), which indicated that when exposed to the NIR-808 nm, UCNP could activate erythrosine, resulting in the production of ROS, which subsequently threatened the survival of bacteria. Figure 2F demonstrates the fluorescence emission profiles of the UCNP and UCSE under 808 nm excitation. From the results, it can be seen that after mesoporous silica modification and loading of erythrosine, the fluorescence intensity of UCSE slightly decreased, which may be caused by the scattering effect of the silica shell layer. The silica inert shell layer blunts the surface of UCNP, which prevents the energy transfer and leads to part of the fluorescence quenching.[35,36] Figure 2G demonstrates the visible-ultraviolet absorption spectra of UCNP@ $mSiO_2$ and UCSE. In UCSE, the loading rate of erythrosine is 22.7%. The release process of erythrosine is shown in Figure S1. The above results indicate that erythrosine was successfully loaded into the core−shell structure of UCNP@ $mSiO_2$.

Next, we used the DPBF molecular probe to detect the generation of $^1O_2$ of UCSE. DPBF is highly specific for $^1O_2$, which can react with it and be consumed, so the generation of $^1O_2$ can be reacted according to the absorption intensity of the characteristic peak of DPBF. Figure 2H demonstrates that the absorbance at 465 nm decreases with time after NIR irradiation for different times, indicating that the $^1O_2$ produced by UCSE excited by NIR is increasing, which suggests that UCSE retains the photodynamic properties of erythrosine and has the potential for photodynamic therapy application.

***In Vitro* PDT Antimicrobial Property.** After the production of ROS by UCSE under NIR excitation was verified, its antibacterial ability was further tested *in vitro*. In this experiment, the bacterial fluids containing or not containing UCSE nanoparticles and whether or not they were in the NIR illumination group were compared with each other, and the PBS bacterial fluids were used as the blank group. The standard plate count method was used to observe the antibacterial activity of UCSE nanoparticles against *E. coli* and *S. aureus*. According to Figure 3A,C, it can be seen that the

https://doi.org/10.1021/acsomega.4c04310
ACS Omega 2024, 9, 34799−34807

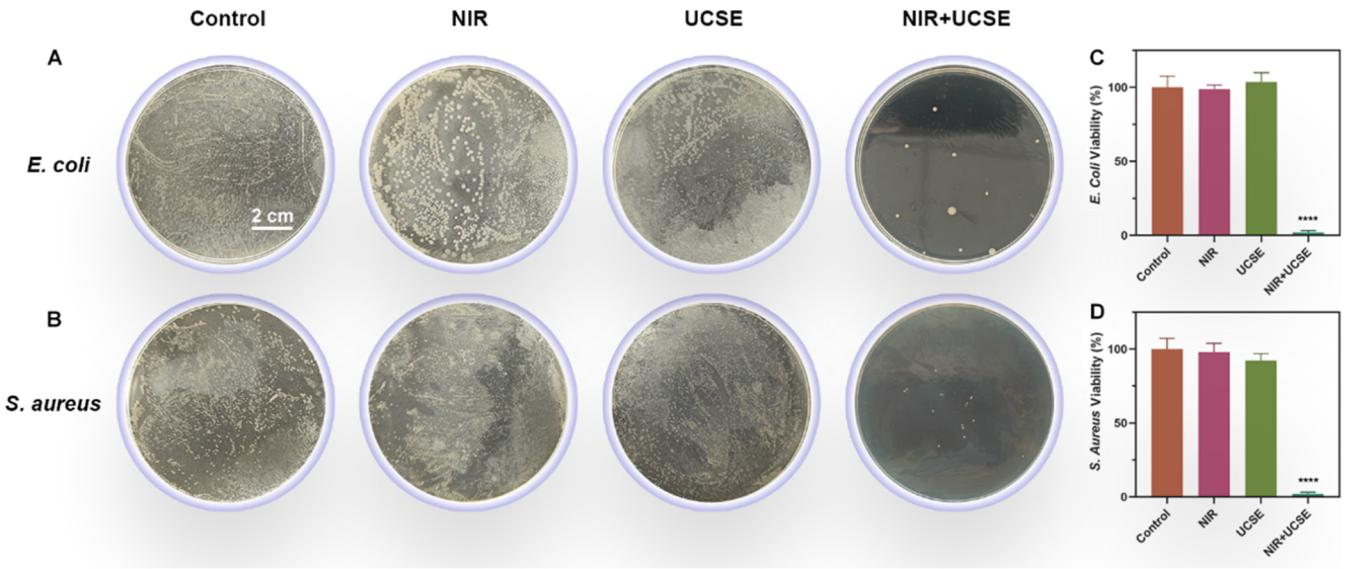

Figure 3. *In vitro* antimicrobial effect of nanoparticles after NIR irradiation. (A, C) Standard plate count images and survival curves of *E. coli* treated with different methodologies. (B, D) Standard plate count images and survival curves of *S. aureus* treated with different methods (scale bar: 2 cm; $n = 3$, $^{****}P < 0.0001$).

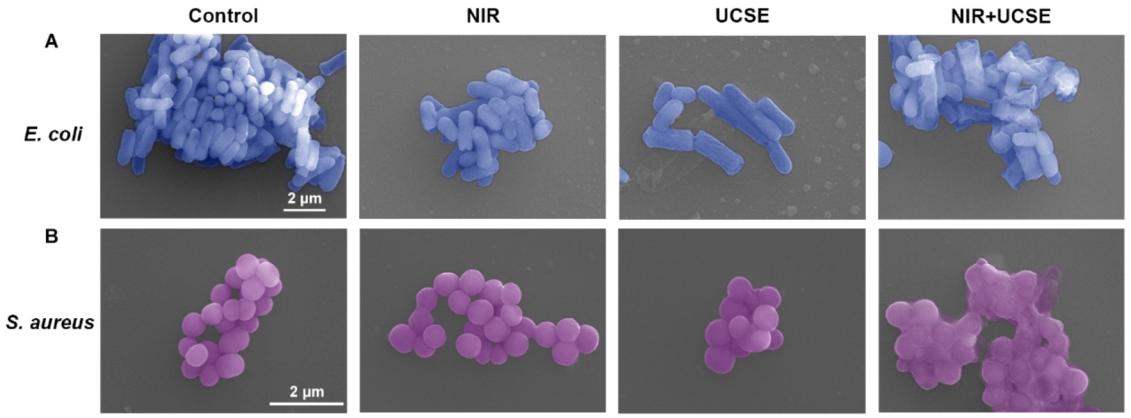

Figure 4. SEM images of (A) *E. coli* and (B) *S. aureus* treated with different methods (scale bar: 2 μm).

number of *E. coli* and the bacterial survival rate of the UCSE group were not significantly lower than those of the PBS group, indicating that the UCSE nanoparticles do not possess antibacterial effects themselves in the absence of NIR-808 excitation. Similar experimental results were observed in the experiments on *S. aureus* (Figure 3B,D). And the colony counts of the UCSE + NIR group were significantly lower than those of the other three groups in both *S. aureus* and *E. coli* antimicrobial experiments. The results of colony counting showed that the antibacterial rate of UCSE could reach 97.41 and 97.69% against *E. coli* and *S. aureus* under NIR-808 nm, respectively (1 W/cm^2 irradiation for 10 min) (Figure 3C,D). In summary, the nanoparticles of UCSE in the UCSE + NIR group showed excellent PDT performance in the bacterial fluid and were able to kill most of the bacteria under NIR irradiation by PDT effect. The other three groups (PBS, NIR, and UCSE groups) did not inhibit the growth of bacteria significantly, because they did not have the ability to generate effective ROS around the bacteria.

Next, we used SEM to observe the bacterial morphology. As shown in Figure 4A, the morphology and size of *E. coli* in the control group could be observed. Under SEM, *E. coli* appeared uniformly cylindrical, with a length of 2−3 μm and a width of 0.5−1 μm, and its shape was complete, with a smooth and defect-free cytosolic wall. *E. coli* treated with UCSE + NIR for 10 min became wrinkled; the continuity of the bacterial cell wall was disrupted, with the cytoplasmic content flowing out, and the morphology of the bacteria became irregular. *S. aureus* in the PBS group was arranged in the shape of grape bunches under SEM, with smooth and intact cell walls and sizes ranging from 0.5 to 1 μm (Figure 4B). However, the appearance of *S. aureus* treated with UCSE + NIR was significantly deformed, and the bacterial size became smaller. In contrast, the bacterial volume sizes of *S. aureus* in the NIR and UCSE groups did not show significant changes.

The antimicrobial ability of UCSE nanoparticles under NIR-808 irradiation can be visualized from the percentage of dead/live bacteria by the fluorescence staining of *E. coli* and *S. aureus* (Figure 5). According to the staining principle, the live bacteria showed green fluorescent dots under the fluorescence microscope, and the PI could not pass through the live cell membrane, only when the cell membrane was damaged, the PI entered the cell, which showed red staining under the fluorescence microscope. The results are shown in Figure

https://doi.org/10.1021/acsomega.4c04310
ACS Omega 2024, 9, 34799−34807

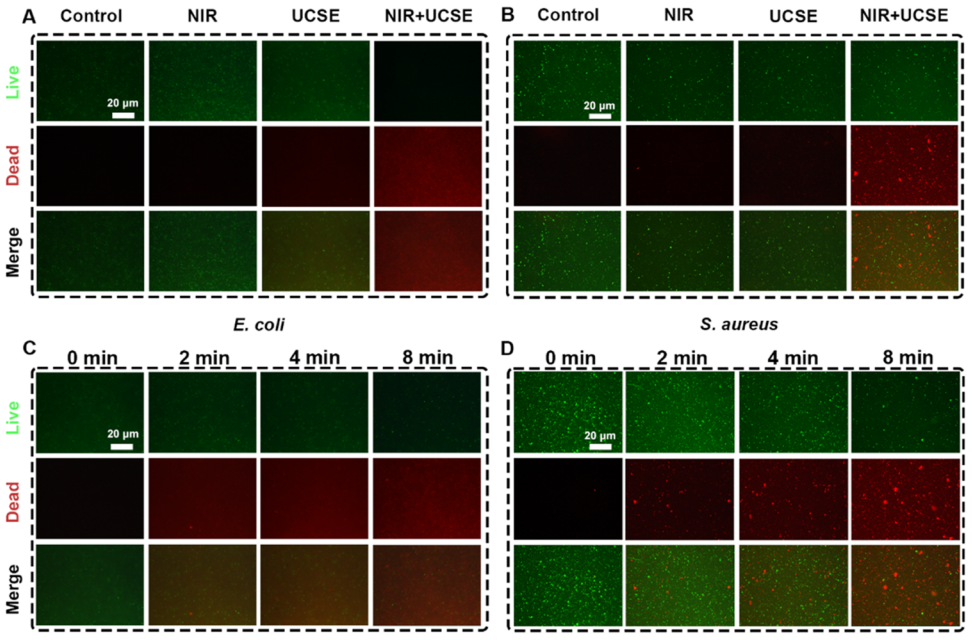

Figure 5. Live/dead staining of *E. coli* and *S. aureus* treated with different methods (A, B) and (C, D) irradiated with NIR-808 nm at different times.

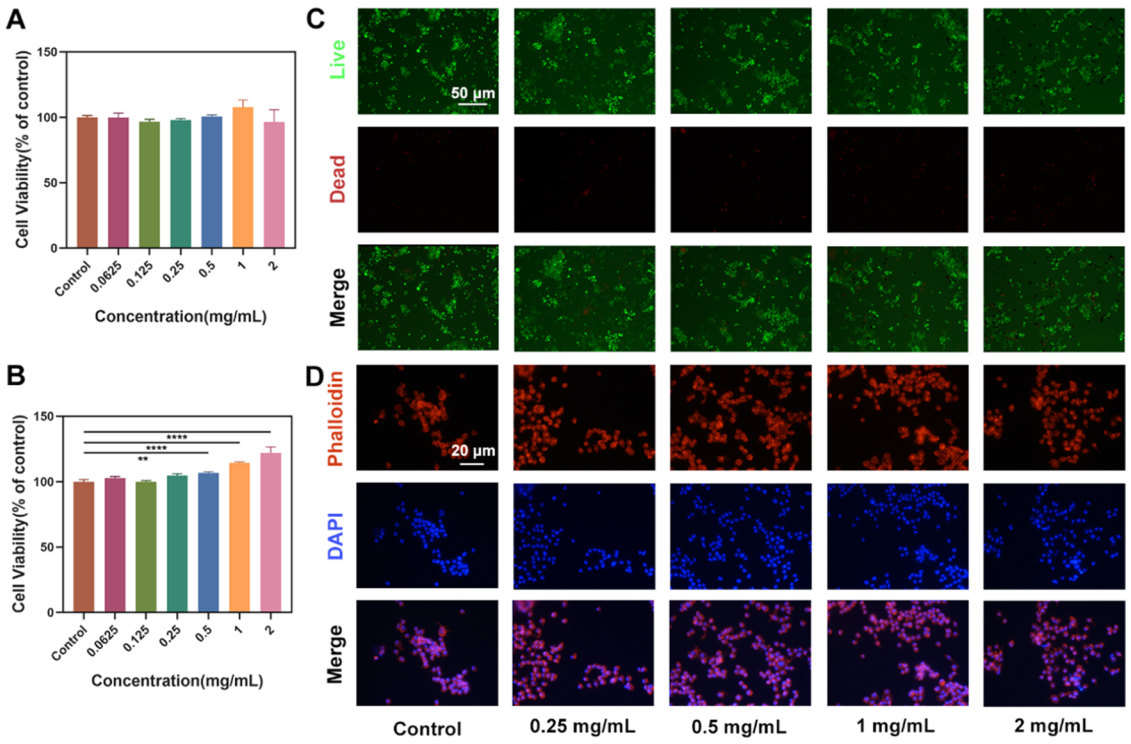

Figure 6. Biosafety analysis *in vitro* of different concentrations of NPs. Viability of RSC96 cells incubated with UCSE NPs for 1 day (A) and 2 days (B). (C) Live- and dead-stained fluorescence images and (D) cytoskeletal staining of RSC96 cells incubated with UCSE at different concentrations.

5A,B, when the green fluorescence is almost not visible in the NIR + UCSE group, while the red fluorescence fills the whole picture, indicating that UCSE can destroy most *E. coli* and *S. aureus* under the excitation of NIR-808 nm, which is consistent with the results of the standard plate count method.

Next, we explored the effect of different irradiation times of NIR-808 nm on the survival states of the two bacteria (Figure 5C,D). When the irradiation time of NIR-808 was 0 min, the vast majority of the green fluorescent dots were visible, and a small portion of them were red fluorescent dots. When irradiated for 2 min, some red fluorescent staining was visible at this time, indicating that some bacteria had died under NIR irradiation. After 4 min of irradiation, the red fluorescent spots further increased. When the light irradiation time reached 8 min, the bacteria were red-stained under the fluorescence microscope, suggesting that almost all of the bacteria died. The above results indicated that the proportion of red fluorescent

https://doi.org/10.1021/acsomega.4c04310
ACS Omega 2024, 9, 34799−34807

dots in *E. coli* and *S. aureus* increased with time and the number of deaths of the two bacteria also increased.

In summary, both *E. coli* and *S. aureus* in the UCSE + NIR group showed different degrees of morphological changes, which suggests that the UCSE + NIR group exerted its antimicrobial effect on *E. coli* and *S. aureus* mainly by destroying the cell membrane and cell wall, which may be related to the large amount of singlet oxygen produced by the UCSE present around the bacteria, which resulted in the bacterial biological activities to be stopping the biological activities of the bacteria, eventually leading to the death of the bacteria.[37,38]

***In Vitro* Cytotoxicity.** Biosafety is the first consideration that needs to be taken into account in solving clinical problems. In this study, the effect of different concentrations of nanoparticles on the viability of RSC96 cells was examined by CCK-8 assay, and the variation of nanoparticles on the morphology of RSC96 was observed by using live−dead cell staining and cytoskeleton. Figure 6A,B shows the cytotoxicity of different concentrations of UCSE (0, 0.0625, 0.125, 0.25, 0.5, 1, and 2 mg/mL) when co-incubated with RSC96 for 1 and 2 days. The results showed that at 1 day of coculture, cell viability was not statistically different from the control even when the nanoparticle concentration was 2 mg/mL. When the coculture time reached 2 days, cell viability increased significantly in the groups with concentrations of 0.5, 1, and 2 mg/mL, and reached 122% when the nanoparticle concentration was 2 mg/mL.

To visualize the changes in cell status, UCSE was cocultured with RSC96 for 1 day and then stained for live and dead cells. Under fluorescence microscopy, green fluorescence represented live cells, and red fluorescence indicated dead cells. As shown in Figure 6C, all groups with different concentrations of UCSE were characterized by predominantly live cells, with no obvious dead cells, which coincided with the CCK-8 results. Next, to observe the effect of nanoparticles on cell morphology, we performed cytoskeletal staining of cells treated with different concentrations. Figure 6D shows that even in the high-concentration state, there was no significant change in cell morphology compared with the control. The above results indicate that UCSE has excellent cell safety for RSC96.

In addition, as shown in Figure S2, under NIR irradiation, the viability of RSC96 cells significantly decreased, indicating that the ROS produced by UCSE poses a threat to cell viability. In fact, current photothermal therapy and photodynamic therapy inevitably have an effect on normal tissues or cells. Therefore, on-demand and responsive treatment methods should become a suitable breakthrough for PDT and PTT: in the case of bacterial infection, photodynamic or photothermal therapy should be used to kill bacteria. After the antibacterial treatment, other active substances loaded could promote the regeneration of surrounding tissues. This treatment approach could minimize the effects of PTT and PDT on normal tissues.

CONCLUSIONS

Overall, we designed and developed UCSE, an efficient antimicrobial PDT platform based on NIR excitation. Under NIR stimulation, UCNP could convert near-infrared light into UV−visible light that could stimulate erythrosine to produce highly efficient ROS, and this noninvasive NIR-triggered strategy realizes more efficient PDT and improves therapeutic efficacy. *In vitro* results showed that UCSE exhibited excellent PDT antimicrobial effects and induced death in *E. coli* and *S. aureus* by disrupting cell membranes. More importantly, UCSE nanoparticles represent promising biosafety materials for clinical applications. Therefore, UCSE is probably an effective alternative to conventional antibiotics and a potential therapeutic strategy for infected skin wounds, periodontitis, and other bacterial infection-like diseases.

ASSOCIATED CONTENT

Supporting Information

The Supporting Information is available free of charge at https://pubs.acs.org/doi/10.1021/acsomega.4c04310.

Photos of erythrosine release in UCSE and cell safety of UCSE under NIR irradiation (PDF)

AUTHOR INFORMATION

Corresponding Author

Qingqing Chen − *Department of Stomatology, Chengdu Seventh People's Hospital (Affiliated Cancer Hospital of Chengdu Medical College), 610041 Chengdu, China*; Email: 394766495@qq.com

Authors

Jing Luo − *Department of Stomatology, Chengdu Seventh People's Hospital (Affiliated Cancer Hospital of Chengdu Medical College), 610041 Chengdu, China*; orcid.org/0009-0008-1601-5596

Hui Zhang − *Department of Stomatology, Chengdu Seventh People's Hospital (Affiliated Cancer Hospital of Chengdu Medical College), 610041 Chengdu, China*

Complete contact information is available at: https://pubs.acs.org/10.1021/acsomega.4c04310

Author Contributions

#J.L. and H.Z. are co-first authors and contributed equally to this work. Methodology, J.L.; software, H.Z.; validation, Q.C.; writing—original draft preparation, J.L.; writing—review and editing, J.L.; visualization, H.Z.; supervision, H.Z. and Q.C.; project administration, Q.C. All authors have read and agreed to the published version of the manuscript.

Funding

This work was supported by the Research project supported by the Joint Research Fund of Chengdu Medical College—Chengdu Seventh People's Hospital [grant number 23LHQYY-01].

Notes

The authors declare no competing financial interest.

ACKNOWLEDGMENTS

The authors thank the department of stomatology for their strong support and the constructive comments of the team members.

REFERENCES

(1) Zhou, B.; Sun, X.; Dong, B.; Yu, S.; Cheng, L.; Hu, S.; Liu, W.; Xu, L.; Bai, X.; Wang, L.; Song, H. Antibacterial PDT nanoplatform capable of releasing therapeutic gas for synergistic and enhanced treatment against deep infections. *Theranostics* **2022**, *12* (6), 2580−2597.

(2) Aminov, R. I. A brief history of the antibiotic era: lessons learned and challenges for the future. *Front. Microbiol.* **2010**, *1*, No. 134.

(3) Friedman, N. D.; Temkin, E.; Carmeli, Y. The negative impact of antibiotic resistance. *Clin. Microbiol. Infect.* **2016**, *22* (5), 416−422.

(4) Shangguan, J.; Wu, Z.; Qiao, C.; Zhang, Y.; Li, L.; Li, Q.; Gao, Y.; Yan, H.; Liu, W. Enhanced Antibacterial Activity against *Escherichia coli* Based on Cationic Carbon Dots Assembling with 5-Aminolevulinic Acid. *ACS Omega* **2024**, *9* (6), 7034−7042.
(5) Tariq, M.; Shivalkar, S.; Hasan, H.; Sahoo, A. K.; Sk, M. P. Manganese Doping in Biomass Derived Carbon Dots Amplifies White Light-Induced Antibacterial Activity. *ACS Omega* **2023**, *8* (51), 49460−49466.
(6) Hu, X.; Zhang, H.; Wang, Y.; Shiu, B.-C.; Lin, J.-H.; Zhang, S.; Lou, C.-W.; Li, T.-T. Synergistic antibacterial strategy based on photodynamic therapy: Progress and perspectives. *Chem. Eng. J.* **2022**, *450*, No. 138129.
(7) Yuan, Z.; Lin, C.; He, Y.; Tao, B.; Chen, M.; Zhang, J.; Liu, P.; Cai, K. Near-infrared light-triggered nitric-oxide-enhanced photodynamic therapy and low-temperature photothermal therapy for biofilm elimination. *ACS Nano* **2020**, *14* (3), 3546−3562.
(8) Kim, H.; Lee, Y. R.; Jeong, H.; Lee, J.; Wu, X.; Li, H.; Yoon, J. Photodynamic and photothermal therapies for bacterial infection treatment. *Smart Mol.* **2023**, *1* (1), No. e20220010.
(9) Wang, W.; Yu, W.; Li, G.; Huang, H.; Song, X.; Yu, L.; Chen, Y. Engineering versatile nano-bacteria hybrids for efficient tumor therapy. *Coord. Chem. Rev.* **2023**, *488*, No. 215178.
(10) Liu, H.; Xing, F.; Zhou, Y.; Yu, P.; Xu, J.; Luo, R.; Xiang, Z.; Rommens, P. M.; Liu, M.; Ritz, U. Nanomaterials-based photothermal therapies for antibacterial applications. *Mater. Des.* **2023**, *233*, No. 112231.
(11) Khan, S.; Rayis, M.; Rizvi, A.; Alam, M. M.; Rizvi, M.; Naseem, I. ROS mediated antibacterial activity of photoilluminated riboflavin: A photodynamic mechanism against nosocomial infections. *Toxicol. Rep.* **2019**, *6*, 136−142.
(12) Jia, Q.; Song, Q.; Li, P.; Huang, W. Rejuvenated photodynamic therapy for bacterial infections. *Adv. Healthcare Mater.* **2019**, *8* (14), No. 1900608.
(13) Chang, W.-Y.; Chen, C.-Y. Antifouling Zwitterionic Nanofibrous Wound Dressing for Long-Lasting Antibacterial Photodynamic Therapy. *ACS Omega* **2023**, *8* (40), 36906−36918.
(14) Zhao, Y.; Hu, M.; Zhang, Y.; Liu, J.; Liu, C.; Choi, S. K.; Zhang, Z.; Song, L. Multifunctional therapeutic strategy of Ag-synergized dual-modality upconversion nanoparticles to achieve the rapid and sustained cidality of methicillin-resistant Staphylococcus aureus. *Chem. Eng. J.* **2020**, *385*, No. 123980.
(15) Krajczewski, J.; Rucińska, K.; Townley, H. E.; Kudelski, A. Role of various nanoparticles in photodynamic therapy and detection methods of singlet oxygen. *Photodiagn. Photodyn. Ther.* **2019**, *26*, 162−178.
(16) Naskar, A.; Kim, K.-s. Friends against the Foe: Synergistic Photothermal and Photodynamic Therapy against Bacterial Infections. *Pharmaceutics* **2023**, *15* (4), No. 1116.
(17) Sikiric, P.; Rucman, R.; Turkovic, B.; Sever, M.; Klicek, R.; Radic, B.; Drmic, D.; Stupnisek, M.; Misic, M.; Vuletic, L. B.; et al. Novel cytoprotective mediator, stable gastric pentadecapeptide BPC 157. Vascular recruitment and gastrointestinal tract healing. *Curr. Pharm. Des.* **2018**, *24* (18), 1990−2001.
(18) Terenzi, A.; Salassa, L. Near-Infrared Photochemistry Assisted by Upconverting Nanoparticles. In *Photoactive Inorganic Nanoparticles*; Elsevier, 2019; pp 43−71.
(19) Kandoth, N.; Barman, S.; Chatterjee, A.; Sarkar, S.; Dey, A. K.; Pramanik, S. K.; Das, A. Photoactive lanthanide-based upconverting nanoclusters for antimicrobial applications. *Adv. Funct. Mater.* **2021**, *31* (43), No. 2104480.
(20) Karimi, M.; Sahandi Zangabad, P.; Baghaee-Ravari, S.; Ghazadeh, M.; Mirshekari, H.; Hamblin, M. R. Smart nanostructures for cargo delivery: uncaging and activating by light. *J. Am. Chem. Soc.* **2017**, *139* (13), 4584−4610.
(21) Nguyen, V.-N.; Zhao, Z.; Tang, B. Z.; Yoon, J. Organic photosensitizers for antimicrobial phototherapy. *Chem. Soc. Rev.* **2022**, *51* (9), 3324−3340.
(22) Wu, S.; Butt, H. J. Near-infrared-sensitive materials based on upconverting nanoparticles. *Adv. Mater.* **2016**, *28* (6), 1208−1226.
(23) Chen, C.; Wang, F.; Wen, S.; Su, Q. P.; Wu, M. C.; Liu, Y.; Wang, B.; Li, D.; Shan, X.; Kianinia, M.; et al. Multi-photon near-infrared emission saturation nanoscopy using upconversion nanoparticles. *Nat. Commun.* **2018**, *9* (1), No. 3290.
(24) Lv, R.; Raab, M.; Wang, Y.; Tian, J.; Lin, J.; Prasad, P. N. Nanochemistry advancing photon conversion in rare-earth nanostructures for theranostics. *Coord. Chem. Rev.* **2022**, *460*, No. 214486.
(25) Li, B.; Ansari, A. A.; Parchur, A. K.; Lv, R. Exploring the influence of polymeric and non-polymeric materials in synthesis and functionalization of luminescent lanthanide nanomaterials. *Coord. Chem. Rev.* **2024**, *514*, No. 215922.
(26) Gonçalves, M. L. L.; Santos, E. M.; Renno, A. C. M.; Horliana, A. C. R. T.; de Almeida Cruz, M.; Parisi, J. R.; Prates, R. A.; Leal-Rossi, A.; Fernandes, K. P. S.; Mesquita-Ferrari, R. A.; Bussadori, S. K. Erythrosine as a photosensitizer for antimicrobial photodynamic therapy with blue light-emitting diodes−An in vitro study. *Photodiagn. Photodyn. Ther.* **2021**, *35*, No. 102445.
(27) Tokubo, L. M.; Rosalen, P. L.; de Cássia Orlandi Sardi, J.; Freires, I. A.; Fujimaki, M.; Umeda, J. E.; Barbosa, P. M.; Tecchio, G. O.; Hioka, N.; de Freitas, C. F.; Terada, R. S. S. Antimicrobial effect of photodynamic therapy using erythrosine/methylene blue combination on Streptococcus mutans biofilm. *Photodiagn. Photodyn. Ther.* **2018**, *23*, 94−98.
(28) Bistaffa, M. J.; Camacho, S. A.; Melo, C. F.; Catharino, R. R.; Toledo, K. A.; Aoki, P. H. Plasma membrane permeabilization to explain erythrosine B phototoxicity on in vitro breast cancer cell models. *J. Photochem. Photobiol., B* **2021**, *223*, No. 112297.
(29) Fracalossi, C.; Nagata, J. Y.; Pellosi, D. S.; Terada, R. S. S.; Hioka, N.; Baesso, M. L.; Sato, F.; Rosalen, P. L.; Caetano, W.; Fujimaki, M. Singlet oxygen production by combining erythrosine and halogen light for photodynamic inactivation of Streptococcus mutans. *Photodiagn. Photodyn. Ther.* **2016**, *15*, 127−132.
(30) Costa, A. C. B. P.; Rasteiro, V. M. C.; Pereira, C. A.; Rossoni, R. D.; Junqueira, J. C.; Jorge, A. O. C. The effects of rose bengal-and erythrosine-mediated photodynamic therapy on Candida albicans. *Mycoses* **2012**, *55* (1), 56−63.
(31) Zhang, T.; Lin, H.; Cui, L.; An, N.; Tong, R.; Chen, Y.; Yang, C.; Li, X.; Liu, J.; Qu, F. Near infrared light triggered reactive oxygen species responsive upconversion nanoplatform for drug delivery and photodynamic therapy. *Eur. J. Inorg. Chem.* **2016**, *2016* (8), 1206−1213.
(32) Grüner, M. C.; Arai, M. S.; Carreira, M.; Inada, N.; de Camargo, A. S. Functionalizing the mesoporous silica shell of upconversion nanoparticles to enhance bacterial targeting and killing via photosensitizer-induced antimicrobial photodynamic therapy. *ACS Appl. Bio Mater.* **2018**, *1* (4), 1028−1036.
(33) Wang, X.-h.; Yu, Y.-x.; Cheng, K.; Yang, W.; Liu, Y.-a.; Peng, H.-s. Polylysine modified conjugated polymer nanoparticles loaded with the singlet oxygen probe 1, 3-diphenylisobenzofuran and the photosensitizer indocyanine green for use in fluorometric sensing and in photodynamic therapy. *Microchim. Acta* **2019**, *186*, No. 842.
(34) Li, B.; Xu, D.; Chen, Y.; Li, W.; Liu, H.; Ansari, A. A.; Lv, R. Polyethylenimine-Coated Pt−Mn Nanostructures for Synergistic Photodynamic/Photothermal/Chemodynamic Tumor Therapy. *ACS Appl. Nano Mater.* **2024**, *7* (8), 9428−9440.
(35) Ling, H.; Guan, D.; Wen, R.; Hu, J.; Zhang, Y.; Zhao, F.; Zhang, Y.; Liu, Q. Effect of Surface Modification on the Luminescence of Individual Upconversion Nanoparticles. *Small* **2024**, *20*, No. 2309035.
(36) Liu, J.-N.; Bu, W.-B.; Shi, J.-L. Silica coated upconversion nanoparticles: a versatile platform for the development of efficient theranostics. *Acc. Chem. Res.* **2015**, *48* (7), 1797−1805.
(37) Muehler, D.; Brandl, E.; Hiller, K.-A.; Cieplik, F.; Maisch, T. Membrane damage as mechanism of photodynamic inactivation using Methylene blue and TMPyP in *Escherichia coli* and *Staphylococcus aureus*. *Photochem. Photobiol. Sci.* **2022**, *21* (2), 209−220.
(38) Rapacka-Zdończyk, A.; Woźniak, A.; Michalska, K.; Pierański, M.; Ogonowska, P.; Grinholc, M.; Nakonieczna, J. Factors

https://doi.org/10.1021/acsomega.4c04310
ACS Omega 2024, 9, 34799−34807

determining the susceptibility of bacteria to antibacterial photodynamic inactivation. *Front. Med.* **2021**, *8*, No. 642609.

https://doi.org/10.1021/acsomega.4c04310
ACS Omega 2024, 9, 34799−34807